

© 2018. This manuscript version is made available under the CC-BY-NC-ND 4.0 license <http://creativecommons.org/licenses/by-nc-nd/4.0/>

## Accepted Manuscript

Title: Nanoscale zero-valent iron-assisted soil washing for the removal of potentially toxic elements

Authors: C. Boente, C. Sierra, D. Martínez-Blanco, J.M. Menéndez-Aguado, J.R. Gallego



PII: S0304-3894(18)30092-X  
DOI: <https://doi.org/10.1016/j.jhazmat.2018.02.016>  
Reference: HAZMAT 19180

To appear in: *Journal of Hazardous Materials*

Received date: 2-11-2017  
Revised date: 24-1-2018  
Accepted date: 5-2-2018

Please cite this article as: Boente C, Sierra C, Martínez-Blanco D, Menéndez-Aguado JM, Gallego JR, Nanoscale zero-valent iron-assisted soil washing for the removal of potentially toxic elements, *Journal of Hazardous Materials* (2018), <https://doi.org/10.1016/j.jhazmat.2018.02.016>

This is a PDF file of an unedited manuscript that has been accepted for publication. As a service to our customers we are providing this early version of the manuscript. The manuscript will undergo copyediting, typesetting, and review of the resulting proof before it is published in its final form. Please note that during the production process errors may be discovered which could affect the content, and all legal disclaimers that apply to the journal pertain.

# Nanoscale zero-valent iron-assisted soil washing for the removal of potentially toxic elements

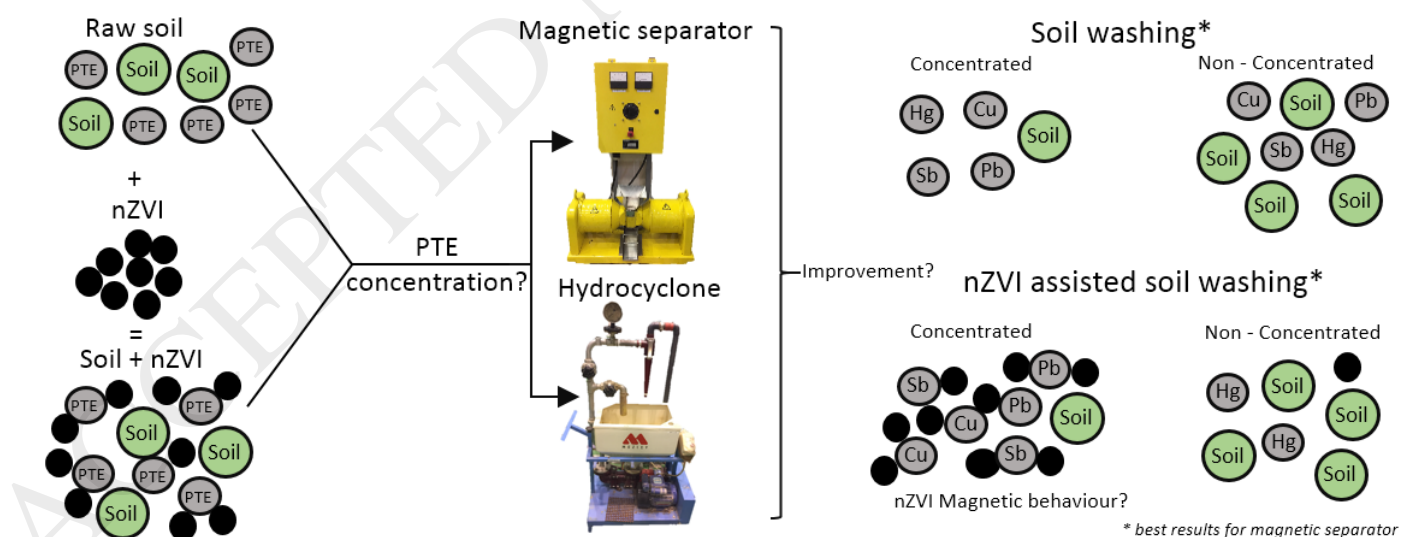
C. Boente<sup>a</sup>, C. Sierra<sup>b</sup>, D. Martínez-Blanco<sup>c</sup>, J.M. Menéndez-Aguado<sup>a</sup>,  
J.R. Gallego<sup>a</sup>

<sup>a</sup> INDUROT and Environmental Biotechnology & Geochemistry Group, University of Oviedo, C/Gonzalo Gutiérrez Quirós s/n, 33600 Mieres (Asturias), Spain.

<sup>b</sup> Escuela Politécnica de Ingeniería de Minas y Energía, University of Cantabria, Boulevard Ronda Rufino Peón no 254, 39316 Torrelavega, Spain.

<sup>c</sup> Servicio Científico-Técnico de Medidas Magnéticas, University of Oviedo, C/Gonzalo Gutiérrez Quirós. s/n, 33600 Mieres, Asturias, Spain.

## Graphical abstract



## Highlights

- Soil washing performance after nZVI addition was examined.
- Dilution effect caused by nZVI was considered for metallurgical accounting purposes.
- Nanoparticle addition improved PTE removal.
- nZVIs were selective for Cu, Pb and Sb.

## Abstract

The present study focuses on soil washing enhancement via soil pretreatment with nanoscale zero-valent iron (nZVI) for the remediation of potentially toxic elements. To this end, soil polluted with As, Cu, Hg, Pb and Sb was partitioned into various grain sizes (500–2000, 125–500 and < 125  $\mu\text{m}$ ). The fractions were pretreated with nZVI and subsequently subjected, according to grain size, to Wet-High Intensity Magnetic Separation (WHIMS) or hydrocycloning. The results were compared with those obtained in the absence of nanoparticles.

An exhaustive characterization of the magnetic signal of the nanoparticles was done. This provided valuable information regarding potentially toxic elements (PTEs) fate, and allowed a metallurgical accounting correction considering the dilution effects caused by nanoparticle addition.

As a result, remarkable recovery yields were obtained for Cu, Pb and Sb, which concentrated with the nZVI in the magnetically separated fraction (WHIMS tests) and underflow (hydrocyclone tests). In contrast, Hg, concentrated in the non-magnetic fraction and overflow respectively, while the behavior of As was unaltered by the nZVI pretreatment. All things considered, the addition of nZVI enhanced the efficiency of soil washing, particularly for larger fractions (125–2000  $\mu\text{m}$ ). The proposed methodology lays the foundations for nanoparticle utilization in soil washing operations.

**Key words:** soil remediation; nanoscale zero-valent iron; soil washing; PTEs

## 1. Introduction

Potentially toxic elements (PTEs) are a major cause of contamination in soils of cities and rural areas. The concept of PTE encompasses a wide selection of elements (As, Cu, Hg, Pb, Zn, among others) that in high concentrations might cause severe damage to the environment and

also to the human health [1,2]. Their persistence in the environment and the ease with which they bioaccumulate and biomagnify in living organisms make them pollutants of special concern [3]. PTEs may derive from natural sources or anthropogenic sources such as mining, industry or traffic [4,5]. In soils they usually appear linked to industrial and chemical waste, or even atmospheric deposition [6]. They enter tissues via ingestion, breathing and touching and cause severe diseases [7]. For all these reasons, their removal has been widely discussed in environmental research over recent decades [8–10].

Of all the remediation techniques available [11], soil washing is widely used [12,13]. It is based on concentrating the contaminants into a reduced volume fraction of the affected soil (or concentrated fraction), thereby leaving the matrix decontaminated (non-concentrated fraction) [14]. The method embraces two contaminant-removal technologies, namely, physical separation, which is based on mineral processing technologies, and chemical extraction, which is based on hydrometallurgy [15].

Here we focused on physical soil washing, that is to say, those procedures that do not alter the chemical properties of materials [12]. In these cases, separation is achieved by means of differences in the physical properties, namely particle size, density, magnetic susceptibility, or even physicochemical properties, as is the case of froth floatation, between the soil and the contaminant [16]. This technique has several advantages, including ease of deployment and versatility to be combined in sequence with other physical and chemical remediation methods [17]. In this context, some researchers have used remediation techniques that combine soil washing together with phytoremediation [18,19], stabilization [20], electrokinetics [21] or ultrasonics [22].

Moreover, the addition of certain compounds such as surfactants [23] and chelants to soil washing enhances PTE recovery [24]. In this respect, nanoscale zero-valent iron (nZVI) is the most commonly used nanomaterial for remediation purposes in Europe and the United States [25,26]. It is a non-toxic reactive metal (as a result of its large surface area, among other factors) that has found wide applications due to its abundance, low cost and ease of production [27]. This remediation material has been successfully applied for the removal of PTEs not only from soils [28–30] but from groundwater [31–34] and water runoff [35].

The applications of nZVI for PTE decontamination of soil are diverse. In this regard, this nanomaterial can be used to immobilize, sorb and capture these compounds [36]. Within this context, nanoparticles enhance soil washing by adsorption of the PTE-containing particles, thereby causing the formation of larger and heavier aggregates which are easier to separate [37]. Regarding magnetic separation, the high magnetic susceptibility of the newly formed aggregates allows the separation of otherwise non-magnetic particles [11,12].

This study aims to evaluate the effect of nZVI as a pre-treatment to a subsequent soil washing process. Thus, the specific objectives were as follows:

- To introduce a procedure that allows the measurement of the amount of natural Fe and nZVI present in each studied fraction.
- To develop a metallurgical accounting correction that circumvents the dilution effect that the addition of nZVI entails, thus facilitating the comparison of results between experiments with and without pretreatments.
- To ascertain the trace elements for which nZVI is selective, on the basis of their behavior in the separation equipment.

## **2. Materials and methods**

### **2.1 Site description and soil sampling**

Soil samples were collected from the old Hg mine of Olicio, in the surroundings of the Picos de Europa National Park (Asturias, Spain). The geology of the area is framed within the Cantabrian zone, specifically in the Ponga mantle [40]. The lithology comprises mainly paraconglomerates, white quartzites and siltstones from the Ordovician period [41]. The first evidence of cinnabar dates back to the late 19<sup>th</sup> century, but it was not until 1965 when underground mining began, persisting until the early 1970s, when the Hg crisis occurred. During these years, the extracted mineral was treated in a retort furnace, and ashes and tailings were mindlessly dumped in the confined valley of the Brengues stream [42].

These mining activities covered approximately 8000 m<sup>2</sup> of the valley with waste, thus enriching the surrounding soils in several PTEs, particularly Hg and As. Within this context, 25 bulk soil samples were collected at a depth of between 0 and 30 cm using a Dutch auger. These samples were then pooled into a single “macro sample” of about 50 kg, which was subsequently sieved through a 2-cm screen to remove rocks, gravel, and other large material.

### **2.2 Soil characterization and chemical analysis**

This macro sample was divided obtaining representative subsamples of 500 g each, which were subjected to wet sieving in order to obtain particle-size fractions of < 125, 125–500 and 500–2000 µm. Thus, normalized sieves were placed in a column, and batches of 100 g of the material were placed in a sieve shaker for 5 min with a water flow of 0.3 l/min (ASTM D-422-63, Standard Test Method for Particle-Size Analysis of Soils). pH was measured with a glass electrode in a suspension of soil and deionized water (1:2.5).

Fractions were then laid out on glass trays, dried at 30°C to prevent Hg volatilization, and finally weighed. Once all the material was meshed, each fraction was split into two equal and representative masses, which were used to perform the experiments with and without nZVI pretreatment.

To standardize the conditions used for chemical determinations, samples > 125 µm were ground in a RS100 Resch mill at 400 rpm for 40 s. Then, 1-g representative subsamples of the diverse origins (soils, grain-size fractions, etc.) were subjected to a 1:1:1 “Aqua regia” digestion. The total concentrations of Ag, Al, As, B, Ba, Bi, Ca, Cd, Co, Cr, Cu, Fe, Ga, Hg, K, La, Mg, Mn, Mo, Na, Ni, P, Pb, S, Sb, Sc, Sr, Th, Ti, Tl, V, W and Zn in the digested material were determined by Inductively Coupled Plasma-Optical Emission Spectroscopy (ICP-OES) at the accredited (ISO 9002) Bureau Veritas Laboratories (Vancouver, Canada).

Powder X-Ray diffraction (PXRD) patterns measured on a PANalytical X’Pert Pro MPD diffractometer with Cu  $k_{\alpha 1}$  radiation (1.540598 Å) were used to determine the mineralogical composition of the soil. After determining the position of Bragg peaks observed over the range of  $2\theta=5-90^\circ$ , the minerals were identified using databases of the International Centre for Diffraction Data.

### 2.3 Nanoscale zero-valent iron pretreatment

A commercial air-stabilized aqueous solution of nZVI (NANOFER STAR-W), supplied by Nano Iron Rajhrad (Czech Republic), was used. This product comprises Fe (0): 14–18%, magnetite ( $\text{Fe}^{2+}\text{Fe}_2^{3+}\text{O}_4^{2-}$ ): 2-6%, carbon (C): 0–1% and about 80% of water. None of these components are classified as hazardous according to 67/548/EEC and Regulation (EC) N° 1278/2008 (CLP). As quoted by the manufacturer, this product is optimal for the preparation of slurries for in-situ remediation purposes [43].

The addition of nanoparticles followed the same procedure for each of the three grain-sizes. Thus, the nZVI drum provided by the manufacturer was first vigorously shaken in order to homogenize and suspend the nanoparticles. Then, 1 l of the homogenized liquid was removed from the barrel and mixed with 100 g of polluted soil. This mixture was stirred for 2 h at 400 rpm. The operation was repeated until 10 l of nanoparticle solution had been mixed with 1000 g of raw soil. This material was then laid in glass trays and air-dried at 30°C in order to prevent nZVI oxidation and Hg evaporation.

Nanoparticles are highly susceptible to oxidation, mainly because of their large surface area. Nonetheless, oxidation was prevented with low drying temperatures and expeditious laboratory experiments. Constant monitoring of the magnetic signal of both soil Fe and nZVI was performed in order to assure the quality of the results.

Soil washing equipment was selected so as to fully exploit the physical properties of nZVI. In this regard, given the high magnetic susceptibility of HIMS, this technique was considered suitable, as was hydrocycloning in the case of the smallest fraction ( $< 125 \mu\text{m}$ ). Experiments were performed with untreated and nZVI-pretreated soils for the three size fractions. Separation tests were performed in triplicate.

## 2.4 Magnetic characterization

To this end, about 100 mg of soil fractions were quartered and ground in an agate mortar in order to be compacted and later encapsulated into an acrylic pillbox. After that, the capsule was fixed to an acrylic rod using double-sided Scotch® tape and placed into the linear motor of a Microsense EV9 vibrating sample magnetometer (VSM). We then measured magnetic hysteresis loops ( $M(H)$ ), which determine magnetization ( $M$ ) as a function of the magnetic field ( $H$ ) in a complete cycle between  $H_{\text{max}} = 20 \text{ kOe}$  and  $H_{\text{min}} = -20 \text{ kOe}$  at room temperature (RT).

Each previous hysteresis loop, defined on the basis of soil grain size and output voltage in the WHIMS, was by pairs corresponding to its mags (magnetically separated fraction) and non-mags (non-magnetically separated fraction) fraction. Thus, the hysteresis loops of each feed (nZVI-pretreated soil samples) were depicted by summing the loops of both the mags and non-mags fractions, which minimized the least-square root difference by means the evolutionary (genetic) method of Microsoft Excel Solver package. In the same manner, the hysteresis loops of each compound (soil treated with nZVI and mags and non-mags fractions) were fitted by adding the corresponding raw soil and pure nZVI, thus determining the percentage of the latter disseminated.

## 2.5 Wet-High Intensity Magnetic Separation

WHIMS is suitable for the treatment of small grain sizes [44]. It is straightforward to use and provides an excellent yield recovery and ratio of concentration [44]. The OUTOTEC Laboratory WHIMS 3X4L apparatus, which has the capacity to separate paramagnetic (weakly magnetic) from non-magnetic materials was used for the experiments.

The feed for the untreated soil was prepared by mixing 50 g of dried soil with 200 g of water (57.5 g in the case of soil pretreated with nZVI, which represents about 16% of Fe (0) and 230 g of water). This slurry was then passed through a matrix canister filled with steel spheres 12.5 mm or 6.5 mm in diameter (depending on the particle-size of the feed; 12.5-mm spheres are appropriate for soil particle sizes  $> 125 \mu\text{m}$ , while 6.5-mm spheres are appropriate for those  $< 125 \mu\text{m}$ ).

The mags material was retained by the magnetized spheres, while the non-mags components and the water passed across the matrix canister and were collected in a tray. Finally, the

magnetic material retained on the spheres was washed out by turning off the equipment, thus reducing the magnetic field to zero.

The variable magnetic field intensity of the equipment was adjusted through the coil input amperage (0-6 amps) [38]. WHIMS was set at 10%, 20%, 30% and 50% of the maximum output voltage for all three fractions (500–2000  $\mu\text{m}$ , 125–500  $\mu\text{m}$  and  $< 125 \mu\text{m}$ ). Higher voltages may render the process economically unviable and may modify the magnetic properties of nZVI. Experiments were performed for untreated and nZVI-pretreated samples. After separation experiments, samples were dried at 30°C, then ground and subsequently subjected to chemical determinations.

## 2.6 Hydrocycloning

The hydrocyclone is one of the most widely used systems for mineral treatment [45]. It separates heavy and light particles via a static piece of equipment that applies a centrifugal force to a liquid (commonly water) that contains the material. This device works in continuous flow mode [46]. The feed to this apparatus is introduced through instantaneous in-flow slurry (feed), which is tangentially pumped inside the cyclone, wherein the joint action of the centrifugal drag and gravity forces separate the particles on the basis of grain size and density [45]. This system determines whether an individual particle flows through the apex (underflow) or the overflow of the hydrocyclone [45], [46]. The underflow and overflow comprise the outflow, the sum of which must be equal to the inflow; the lighter and finer particles report to the overflow.

Regarding the current study, a hydrocycloning lab-scale plant (C700 Mozley) with a capacity to operate hydrocyclones from 10 to 50 mm in diameter was used. The solid:water ratio of the slurry feed used in the experiments was constant (1:5), whereas the apex diameters (9.5 mm and 6.5 mm) and working pressures (69 and 138 kPa) were combined (e.g. [47]). The procedure was used to treat the grain size fraction  $< 125 \mu\text{m}$ , in accordance with the manufacturer's specifications. In all cases, after reaching a stationary regime, samples from the underflow and overflow were collected in borosilicate flasks and then weighed. Thereafter, they were dried at 30°C, and representative subsamples were obtained for chemical determinations. Tests were performed in triplicate.

## 2.7 Evaluation of results

### 2.7.1 Corrected expressions for weight and element recoveries

The efficiency of the concentration operation was evaluated in terms of two concepts, namely weight recoveries and element recoveries [14]. Both concepts can be referred to any outflow from the WHIMS and hydrocyclone, irrespective of whether they correspond to the concentrated or non-concentrated fractions [48]. Nevertheless, all calculations in this study refer



to the concentrated fraction, that is to say, the fraction in which element recovery was higher than weight recovery. In this case, this refers to the magnetic fraction of the WHIMS and the overflow of the hydrocyclone.

The concepts of weight recovery (WR) and element recovery (ER) used in this study were as defined by Wills [15]. These expressions are valid for any soil without nZVI pre-treatment, but nanoparticle addition entails a dilution effect that makes the correction of the abovementioned equations necessary in terms of facilitating the comparison of results between experiments with and without pretreatments. In this respect, considering that the original amount of Fe of the soil was small (between 0.9–2.6% Fe, see Table 1) compared with that after nZVI pretreatment, the dilution effect was removed by subtracting the weight of Fe. Thus, the corrected weight recovery in the concentrated fraction ( $WR_c'$ ) would be:

$$WR_c' = \frac{w_c - w_c^{Fe}}{w_c + w_{nc} - w_c^{Fe} - w_{nc}^{Fe}} \quad (1),$$

where  $w_c$  is the weight of the concentrated fraction and  $w_{nc}$  the weight of the non-concentrated fraction,  $w_c^{Fe}$  and  $w_{nc}^{Fe}$  being the weight of Fe in these fractions respectively. The  $WR_{nc}'$  is calculated similarly.

The concentration of the other elements is also altered when the weight of Fe is removed, but this change does not appreciably affect the comparability of the results. The corrected masses of element “i” in the concentrated ( $w_c^i$ ) and non-concentrated ( $w_{nc}^i$ ) fractions,  $[i_c]$  and  $[i_{nc}]$  being the concentration of the element “i” in the concentrated fraction, can be calculated as:

$$w_c^i = WR_c' \cdot [i_c] \quad (2)$$

$$w_{nc}^i = WR_{nc}' \cdot [i_{nc}] \quad (3),$$

where  $[i_c]$  and  $[i_{nc}]$  is the concentration of element “i” in the concentrated or non-concentrated fraction respectively.

Finally, once  $w_c^i$  and  $w_{nc}^i$  have been calculated, the corrected element enrichment factor ( $ER_c^i$ ) for element “i” can be obtained as follows:

$$ER_c^{i'} = \frac{w_c^{i'}}{w_c^{i'} + w_{nc}^{i'}} \quad (4).$$

### 2.7.2 Determination of nZVI fate by magnetic quantification

The magnetization of the WHIMS feed ( $M_s$ ) corresponding to the original soil treated with nZVI, i.e. the blend of soil and nanoparticles obtained in the stirring tank before the separation test, was estimated using a linear combination of the measured signal of the original soil fraction (not treated with nanoparticles, denoted as  $M^0$ ) and the signal of the pure nZVI ( $M^{nZVI}$ ). Thus, the magnetization for the mixture in a magnetic field, “i”, can be calculated as:

$$M_s(H_i) = \%_s^{nZVI} \cdot M^{nZVI}(H_i) + (1 - \%_s^{nZVI}) \cdot M^0(H_i) \quad (5),$$

where the common factor,  $\%_s^{nZVI}$ , which minimizes the sum of square root difference between the two members for all applied magnetic fields “i” of the M(H) curve, represents the weight percentage of nZVI in the WHIMS feed. Likewise, once all the tests had been performed, magnetization values for the mags ( $M_M$ ) and non-mags ( $M_{NM}$ ) fractions were also modeled using analogous equations as follows:

$$\begin{aligned} M_M(H_i) &= \%_M^{nZVI} \cdot M^{nZVI}(H_i) + (1 - \%_M^{nZVI}) \cdot M^0(H_i) \\ M_{NM}(H_i) &= \%_{NM}^{nZVI} \cdot M^{nZVI}(H_i) + (1 - \%_{NM}^{nZVI}) \cdot M^0(H_i) \end{aligned} \quad (6),$$

$\%_M^{nZVI}$  and  $\%_{NM}^{nZVI}$  being the weight % of nZVI in the mags and non-mags fractions, respectively.

On the other hand, signals from the mags ( $M_M$ ) and non-mags ( $M_{NM}$ ) fractions were also used to reconstruct the previous feed signal ( $M_s$ ) for each test. In this case, the least-square root fit of data was derived as:

$$M_s(H_i) = \%_M \cdot M_M(H_i) + (1 - \%_M) M_{NM}(H_i) \quad (7),$$

where  $\%_M$  is the proportion of magnetics in the mags. Finally, by combining equations (6) and (7), we can also calculate the weight percentage of nZVI in the feed belonging to each pair of mags and non-mags fractions, by means of:

$$\%_s^{nZVI} = \%_M \cdot \%_M^{nZVI} + (1 - \%_M) \cdot \%_{NM}^{nZVI} \quad (8).$$

### 3. Results and discussion

#### 3.1 Textural and chemical characterization of the soil

X-ray diffraction results (Figure 1) indicated that the soil samples were composed mainly of quartz ( $\text{SiO}_2$ ), some calcite ( $\text{CaCO}_3$ ), and muscovite ( $\text{KAl}_2(\text{AlSi}_3\text{O}_{10})(\text{OH})_2$ ), and probably also hematite ( $\text{Fe}_2\text{O}_3$ ), with an unclear presence of dolomite ( $\text{CaMg}(\text{CO}_3)_2$ ) and microcline ( $\text{KAlSi}_3\text{O}_8$ ). Table 1 shows the element concentrations for the different grain sizes. pH values measured were slightly alkaline (around 7.5).

The coarser fraction ( $> 2000 \mu\text{m}$ ) accounted for approximately 50%<sub>w</sub> of the bulk soil, followed by the fine fraction ( $< 125 \mu\text{m}$ ), which accounted for roughly 26%<sub>w</sub>. The 500–2000  $\mu\text{m}$  and 125–500  $\mu\text{m}$  fractions represented 11%<sub>w</sub> and 12%<sub>w</sub> respectively. The main potential toxicant in the bulk samples was Hg and to a lesser extent As, Cu and Sb. In the  $< 125 \mu\text{m}$  fraction, Pb played an important role.

Chemical determinations revealed that the abovementioned elements were the main environmental threats in the soil. However, the presence of other elements may indicate how they interact with other soil constituents. We therefore also included the following in our analysis: Al as representative of clays; Ca of carbonates; K of feldspars; La and Y of rare earth; V as neutral element (does not associate to any other); and Fe (main component of the nanoparticles).

#### 3.2 Metallurgical accounting

First, corrected weight and element recoveries were calculated in order to compare the efficiency of soil washing with and without the nZVI pretreatment. The results corresponding to the WHIMS are shown in Table 2.

As can be observed, weight recoveries showed great variations after nZVI pretreatment. Thus, classical soil washing yielded corrected weight recoveries ranging from 3% to 20% in the concentrated fraction, whereas values for the pretreated soil ranged from 30% to 76%. In both cases, the greater the output voltage, the larger the weight recovery obtained. Simultaneously, higher voltages provided a slight improvement in element recoveries. In this respect, an increase in field intensity has to be seen as a trade-off between the previous facts, as well as the subsequent larger weight recovery in the concentrated fraction and higher power consumption.

Regarding the corrected element recoveries, significant improvement after nZVI pretreatment was achieved for all the elements studied. It is important to indicate that all element recoveries were corrected to minimize the effect of nanoparticle addition on the comparability of results with those of untreated samples. In this respect, Fe recovery was greatly increased for the nZVI-

assisted concentration experiments as recoveries for this element cannot be corrected by subtracting the concentration of Fe.

It must be indicated that element recoveries rose in parallel to weight recovery. Since the aim of the concentration operation is to achieve high element recoveries for the smallest possible weight recoveries, a new trade-off between the two variables has to be established. This optimum could possibly be at around 30% of the maximum output voltage.

The best results in grain-size terms were obtained for the pretreated 500-2000  $\mu\text{m}$  fraction (Table 2), with significantly high recoveries of Cu (> 90%), Pb (> 80%) and Sb (60-70%). Results were similar for the pretreated 125-500  $\mu\text{m}$  fraction, Cu being the element with the greatest recovery (around 90%) for a repeatable mass of soil (30–40%). The previous experiments did not present appropriate concentration yields for the < 125  $\mu\text{m}$  fraction. Therefore, a set of hydrocycloning tests was performed for this fraction (Table 3).

As occurred for the WHIMS assays, the immediate effect of nZVI pretreatment was an increase in weight and element recovery. However, although the pretreatment produced remarkable improvements in the hydrocycloning of this fraction (< 125  $\mu\text{m}$ ), the results were more modest than those of WHIMS. In this regard, smaller apex diameters translated into greater recoveries, although an increase in operating pressure did not lead to appreciable variations but may result in greater equipment abrasion. All things considered, although the performance of the separator was enhanced after nZVI pretreatment and certain selectiveness over Pb, Cu and Sb was observed, element recoveries as compared to weight recoveries were not as remarkable as in the WHIMS device, thus indicating poorer upgrading. These results are further discussed in the next section.

### 3.3 Nanoscale zero-valent Fe selectivity

nZVI Fe selectivity with regard to PTEs can be easily visualized by plotting  $ER_c^i$  vs.  $WR_c'$  and determining the separation between the represented points from the perfect splitting line ( $ER_c^i = WR_c'$ ). Thus, points along this line are undesirable since separation does not take place and, conversely, the further the distance of a point from the “perfect splitting” line, the better the concentration levels obtained.

Moreover, this line divides the figures into two triangles. The one on the top is the domain of the concentrated elements, that is to say, those elements that tend to accumulate in the mags fraction (WHIMS) or the overflow (hydrocyclone). In contrast, the area below the perfect splitting line comprises the elements that tend to accumulate in the non-mags fraction or in the underflow.

#### 3.3.1 Wet-High Intensity Magnetic Separation

In all experiments (Figures 2, 3 and 4) there are two clusters of points, the left one (circles) corresponding to traditional soil washing tests and the right one (crosses) to the nZVI-enhanced tests. Both clusters are clearly separated, thereby indicating that the addition of nanoparticles had a strong effect on the separation. Moreover, more elements scattered from the non-concentration line after nZVI pretreatment, thus revealing that the addition of this nanomaterial enhances concentration.

By size intervals, in the 500-2000  $\mu\text{m}$  fraction (Figure 2), nZVI pretreatment enhanced Cu, Pb and Sb concentration in the mags fraction and Hg in the non-mags fraction; while As showed better yields in the untreated tests than under nZVI pretreatment. Moreover, Al, K, and La and Y, representative of clays, feldspars, rare earth, respectively and which were not concentrated in the mags fraction by traditional soil washing, concentrated in the non-mags fraction after addition of nZVI. Conversely, Ca, which is generally prone to concentrating in the non-mags fraction, lost this tendency. Finally, V seemed unaffected by nZVI pretreatment.

The 125–500  $\mu\text{m}$  fraction (Figure 3) showed similar results. Thus, Cu yielded better concentrations, as did Sb and Pb after pretreatment with nanoparticles. Note that all the PTEs accumulated in the mags fraction, with the exception of Hg, which was markedly concentrated in the non-mags fraction with other elements such as Al and rare earths. This observation suggests that nZVI repels Hg-containing particles (mostly of cinnabar).

The thickest fraction ( $< 125 \mu\text{m}$ ) presented several differences with regards to the preceding ones (Figure 4). Thus, it was difficult to concentrate any of the elements, the only exception being Cu. This observation could be explained as magnetic forces can be overcome by dragging forces for the smallest grain sizes [39]. Despite this drawback, the positive effects of nZVI on separation were once again observed.

All things considered, we conclude that the nanoparticles were selective for Cu, Pb and Sb in the 125–2000  $\mu\text{m}$  size range. Moreover, Hg was also concentrated in this size interval but in the non-mags fraction. As regards the  $< 125 \mu\text{m}$  fraction, a certain degree of selectivity was observed but the separation efficiency diminished with grain size.

A proper discussion on PTEs mobility in soils is complex and commonly associated with adsorption and desorption processes as well as to precipitation with Al, Fe and Mn oxides (e.g.: [49,50]). In this context, in our case, we hypothesized the relevance of the amount of magnetite in the nanoparticles applied. In general, iron oxides adsorption capacities are greatly influenced by the redox conditions, the presence of other ions and the pH. Particularly, adsorption mechanisms of metals on magnetite are mainly due to the electrostatic attraction between the metallic ions and nanoparticles, being the hydrated ionic radius of cations a key parameter [51]. Magnetite is an amphoteric solid which may adsorb either negatively or positively charged

species depending on pH variations. Magnetite surface has a positive charge at pH below 6.7-7 with prevalence of  $\text{FeOH}^{2+}$  on its surface, and negative when the pH is higher and groups  $\text{FeO}^-$  are predominant [15]. As a consequence, for most PTEs (metals), magnetite adsorption efficiency increases with rising pH because they are prone to be in cationic form; on the contrary, As is mostly present in the form of oxyanions [51,52] when the pH is slightly alkaline as occur in this work.. Therefore, As behavior is different, as electrostatic repulsion between the arsenates and magnetite (with a net negative charge) hinders adsorption [53]. Moreover, As could co-precipitate with Fe (III) ions forming amorphous Fe arsenates and secondary oxidation minerals [54]. On the whole, maximum adsorption capacity of As on Fe oxides may occur at pH between 4 and 6 [55–57]. In addition, it has to be also pointed out that reliable adsorption determinations are complex at neutral or alkaline pH as a consequence of cations precipitation as hydroxides [51].

Concerning the preference of Hg for the non-mags fraction, it has to be considered that in the studied soil the Hg predominant form is cinnabar [48]. This mineral has mainly on its surface exposed hydroxyl sites and sulfide groups [58] which are negatively charged at pH above 3-4 [59] thus hindering sorption on magnetite surface.

### 3.3.2 Hydrocyclone

Given the unsatisfactory concentration yields obtained for the  $< 125 \mu\text{m}$  fraction, hydrocycloning was also tested. In this respect, a hydrocycloning test without nZVI pretreatment did not provide a significant improvement in separation yields. Moreover, samples pretreated with nZVI did not show a clear separation of elements, with all the points placed near or along the perfect splitting line and untreated and pretreated point clusters located very close as shown in Figure 5.

In this respect, it must be commented that Cu was concentrated only when the nZVI particles were added. This observation suggests that the hydrocyclone showed less effectiveness as a concentrator compared with WHIMS even under nZVI pretreatment conditions. Regarding the interaction of nanoparticles with the PTEs, the positions of Cu and Hg showed variations with respect to the non-concentration line, as occurred for WHIMS, thereby evidencing that nZVI preferentially interacts with these two elements.

## 3.4 Magnetic quantifications

### 3.4.1 Magnetic signals of the nZVI, soil and feeds

Figure 6 shows the hysteresis loops of: a) pure nZVI, b) raw soil and c) nZVI-pretreated soil when fed to the separating apparatus. Each hysteresis loop is depicted on the basis of soil grain-size: 500–2000  $\mu\text{m}$  (blue), 125–500  $\mu\text{m}$  (green) and < 125  $\mu\text{m}$  (red).

In this respect, a relative low difference in magnetic susceptibility (below 0.5%) was observed in pure nZVI, as reflected by identical shape of the curves (Figure 6a). This observation suggests that the distribution of the nanoparticles in the feed was homogeneous. Moreover, the hysteresis loops of the raw soil samples differed considerably in terms of both maximum magnetization value and form, with signals approximately 1/400-1/1000 smaller than those registered for pure nZVI (Figure 6b).

The medium fraction of the raw soil had a significantly smaller magnetic signal, while the larger fraction had the highest signal (Figure 6b). Once the nZVI was added, the red line became the most prominent, thereby revealing that the < 125  $\mu\text{m}$  grain-size fraction had the highest proportion of nZVI (Figure 6c). Moreover, this figure evidences that aggregation of nZVI in the soil was heterogeneous, as curves showed different shapes and magnetic signals.

All things considered, the linear combination of the pure nZVI signal and that of the raw soil (Equation 5) allowed the reconstruction of nZVI concentration in each feed. Thus, the magnetic signals indicated higher concentration for the finest grain size (18.52% < 125  $\mu\text{m}$ ), intermediate for the largest grain size (16.50%, 500–2000 $\mu\text{m}$ ) and lower for the medium grain size (11.27%, 125–500  $\mu\text{m}$ ). These results highlight how nanoparticle coalescence hinders the achievement of a homogenous soil-nanoparticle mixture.

Once the concentration experiments were completed, the magnetic signals of the mags and non-mags fractions were measured and the magnetic signal of the feed was reconstructed using equation 6. Figures 7 and 8 show the signals of the two separated fractions (mags and non-mags) for all the experiments.

Regarding the hysteresis loops of the mags fraction, the maximum signal (corresponding to the highest concentration of nZVI) was obtained for the 500–2000  $\mu\text{m}$  and 125–500  $\mu\text{m}$  fractions at 30% of the maximum output voltage (Figure 7, column C). When chemical analyses were taken into consideration, the highest element recoveries for relatively low weight recoveries were also obtained for this voltage. High element recoveries at this voltage suggest that nZVI acted as a PTE scavenger, as PTE recovery was related to the recovery of nZVI. This observation is also confirmed by the finding that the greater the magnetization (or nanoparticle content), the higher the recovery of Cu, Pb and Sb for a fixed grain size (Figure 7, rows A', B' and C').

Furthermore, as shown in B' and C', increasing the maximum output voltage over 30% did not promote nZVI recovery—and subsequently more PTEs—in the mags fraction. Conversely, the magnetization for the < 125  $\mu\text{m}$  fraction was minor at 30% voltage. This observation is

consistent with previous findings (section 3.2), in which it was concluded that the metallurgical accounting revealed problems with the separation for this size. In fact, concerning the magnetic signals, these problems in the thickest fractions are also reflected in terms of the difference between the  $< 125 \mu\text{m}$  signals and the respective  $500\text{--}2000 \mu\text{m}$  and  $125\text{--}500 \mu\text{m}$ . In any case, for each experiment, almost all the nZVI was concentrated in the magnetic part (as revealed by the low percentages of nZVI in non-mags loops), thereby confirming a correlation between the accumulation of Cu, Pb, Sb in the mags fraction (or Hg in the non-mags fraction).

Additionally, Figure 8 shows the signals of the non-mags for all the experiments. In this case it can be appreciated that the percentage of nZVI is lower than 1% in all the cases, evidencing that nZVI tends to accumulate in the magnetic fractions (Figure 7). Moreover, this percentage decreases as the intensity of the magnetic field rises.

Finally, the ratio  $\%_s^{\text{nZVI}}$  (i.e.; the percentage of nZVI in the soil feed) was calculated by means of equation 8, providing similar concentrations to those reconstructed with equation 5, as can be seen in Table 4. This ratio is a way of checking the robustness of the method of mixing and the innovative formulation presented.

## 4. Conclusions

Here we studied the effect of nZVI as a pretreatment to a subsequent soil washing process of soil affected by PTEs. To this end, various grain-size fractions were pretreated with nZVI and subjected to WHIMS or hydrocycloning. The study included an exhaustive chemical and magnetic characterization.

We introduced a correction of element recoveries in order to facilitate the comparison of results from experiments with and without nZVI pretreatment. In this respect, the equations proposed provided coherent results and successfully removed the dilution effect caused by nZVI addition.

Nanoparticle pretreatment performed before WHIMS provided satisfactory results, improving PTE concentrations for the  $125\text{--}500 \mu\text{m}$  and  $500\text{--}2000 \mu\text{m}$  grain-size fractions. However, concentration by hydrocycloning and WHIMS presented problems for the  $< 125 \mu\text{m}$  fraction.

On the basis of these experiments, we conclude that nZVI preferentially interacts with Cu, Sb and Pb (making them report to the mags fraction) and Hg (which reported to the non-mags fraction). Unlike the previous elements, nanoparticles did not have a clear effect on As concentration.

Concerning the magnetic signals study, the hysteresis loops and proposed equations allowed us to determine the amount of nanoparticles present in each of the separated fractions. These



results were essential to corroborate the contribution of nZVI to enhancing the concentration process, as well as to perform the metallurgical accounting correction. In this respect, we conclude that the larger the nZVI dose, the better the PTE recovery. Along the same lines, optimal operating conditions were deemed to be at 30% of the maximum output voltage, except in the < 125  $\mu\text{m}$  fraction. In view of the aforementioned findings, we conclude that nZVI treatment prior to soil washing brings about an improvement in PTE recovery.

### Acknowledgements

This work was supported by Project CTM2016-75894-P (MINECO). Carlos Boente obtained a grant from the “Formación del Profesorado Universitario” program, financed by the “Ministerio de Educación, Cultura y Deporte de España”. The authors thank the “Servicio Científico-Técnico de Medidas Magnéticas” of the University of Oviedo.

## 5. References

- [1] M. Biasioli, H. Grčman, T. Kralj, F. Madrid, E. Díaz-Barrientos, F. Ajmone-Marsan, Potentially toxic elements contamination in urban soils: a comparison of three European cities., *J. Environ. Qual.* 36 (2007) 70–9. doi:10.2134/jeq2006.0254.
- [2] C. Huamain, Z. Chunrong, T. Cong, Z. Yongguan, Heavy Status Metal and in China : in *Soils Pollution Countermeasures*, *Ambio.* 28 (1999) 130–134.
- [3] S. Clemens, Toxic metal accumulation, responses to exposure and mechanisms of tolerance in plants., *Biochimie.* 88 (2006) 1707–19. doi:10.1016/j.biochi.2006.07.003.
- [4] C.L.S. Wiseman, F. Zereini, W. Püttmann, Traffic-related trace element fate and uptake by plants cultivated in roadside soils in Toronto, Canada, *Sci. Total Environ.* 442 (2013) 86–95. doi:10.1016/j.scitotenv.2012.10.051.
- [5] C. Boente, N. Matanzas, N. García-González, E. Rodríguez-Valdés, J.R. Gallego, Trace elements of concern affecting urban agriculture in industrialized areas: A multivariate approach, *Chemosphere.* 183 (2017) 546–556. doi:10.1016/j.chemosphere.2017.05.129.
- [6] A. Kabata-Pendias, *Trace elements in soils and plants*, 2011. doi:10.1201/b10158-25.

- [7] L. Järup, Hazards of heavy metal contamination, *Br. Med. Bull.* 68 (2003) 167–182. doi:10.1093/bmb/ldg032.
- [8] M. Farrell, D.L. Jones, Use of composts in the remediation of heavy metal contaminated soil, *J. Hazard. Mater.* 175 (2010) 575–582. doi:10.1016/j.jhazmat.2009.10.044.
- [9] V.R. Ouhadi, R.N. Yong, N. Shariatmadari, S. Saeidijam, A.R. Goodarzi, M. Safari-Zanjani, Impact of carbonate on the efficiency of heavy metal removal from kaolinite soil by the electrokinetic soil remediation method, *J. Hazard. Mater.* 173 (2010) 87–94. doi:10.1016/j.jhazmat.2009.08.052.
- [10] A.M. Jiménez-Rodríguez, M.M. Durán-Barrantes, R. Borja, E. Sánchez, M.F. Colmenarejo, F. Raposo, Heavy metals removal from acid mine drainage water using biogenic hydrogen sulphide and effluent from anaerobic treatment: Effect of pH, *J. Hazard. Mater.* 165 (2009) 759–765. doi:10.1016/j.jhazmat.2008.10.053.
- [11] R. a. Wuana, F.E. Okieimen, Heavy Metals in Contaminated Soils: A Review of Sources, Chemistry, Risks and Best Available Strategies for Remediation, *ISRN Ecol.* 2011 (2011) 1–20. doi:10.5402/2011/402647.
- [12] G. Dermont, M. Bergeron, G. Mercier, M. Richer-Lafleur, Soil washing for metal removal: A review of physical/chemical technologies and field applications, *J. Hazard. Mater.* 152 (2008) 1–31. doi:10.1016/j.jhazmat.2007.10.043.
- [13] K.K. Fedje, L. Yillan, A.M. Strömvall, Remediation of metal polluted hotspot areas through enhanced soil washing - Evaluation of leaching methods, *J. Environ. Manage.* 128 (2013) 489–496. doi:10.1016/j.jenvman.2013.05.056.
- [14] C. Sierra, J.R. Gallego, E. Afif, J.M. Menéndez-Aguado, F. González-Coto, Analysis of soil washing effectiveness to remediate a brownfield polluted with pyrite ashes., *J. Hazard. Mater.* 180 (2010) 602–8. doi:10.1016/j.jhazmat.2010.04.075.
- [15] B. Wills, J. Finch, *Mineral Processing Technology: An Introduction to the Practical Aspects of Ore Treatment and Mineral Recovery*, 2015. doi:10.1016/B978-075064450-1/50003-5.
- [16] R.J. Abumaizar, E.H. Smith, Heavy metal contaminants removal by soil washing, *J. Hazard. Mater.* 70 (1999) 71–86. doi:10.1016/S0304-3894(99)00149-1.
- [17] H. Freeman, E. Harris, *Hazardous waste remediation: innovative treatment technologies*, 1995.
- [18] M. Sung, C.Y. Lee, S.Z. Lee, Combined mild soil washing and compost-assisted phytoremediation in treatment of silt loams contaminated with copper, nickel, and

- chromium, *J. Hazard. Mater.* 190 (2011) 744–754. doi:10.1016/j.jhazmat.2011.03.113.
- [19] A. Komínková, D., Fabbicino, M., Gurung, B., Race, M., Tritto, C., & Ponzo, Sequential application of soil washing and phytoremediation in the land of fires, *J. Environ. Manage.* 206 (2018) 1081–1089. doi:10.1016/j.jenvman.2017.11.080.
- [20] X. Yoo, J. -, Beiyuan, J., Wang, L., Tsang, D. C. W., Baek, K., Bolan, N. S., . . . Li, A combination of ferric nitrate/EDDS-enhanced washing and sludge-derived biochar stabilization of metal-contaminated soils, *Sci. Total Environ.* 616–617 (2018) 572–582. doi:10.1016/j.scitotenv.2017.10.310.
- [21] K.R. Reddy, K. Maturi, C. Cameselle, Sequential Electrokinetic Remediation of Mixed Contaminants in Low Permeability Soils, *J. Environ. Eng.* 135 (2009) 989–998. doi:10.1061/(ASCE)EE.1943-7870.0000077.
- [22] B. Park, Y. Son, Ultrasonic and mechanical soil washing processes for the removal of heavy metals from soils, *Ultrason. Sonochem.* 35 (2017) 640–645. doi:10.1016/j.ultsonch.2016.02.002.
- [23] L.G. Torres, R.B. Lopez, M. Beltran, Removal of As, Cd, Cu, Ni, Pb, and Zn from a highly contaminated industrial soil using surfactant enhanced soil washing, *Phys. Chem. Earth.* 37–39 (2012) 30–36. doi:10.1016/j.pce.2011.02.003.
- [24] A. Giannis, A. Nikolaou, D. Pentari, E. Gidarakos, Chelating agent-assisted electrokinetic removal of cadmium, lead and copper from contaminated soils, *Environ. Pollut.* 157 (2009) 3379–3386. doi:10.1016/j.envpol.2009.06.030.
- [25] E. Lefevre, N. Bossa, M.R. Wiesner, C.K. Gunsch, A review of the environmental implications of in situ remediation by nanoscale zero valent iron (nZVI): Behavior, transport and impacts on microbial communities, *Sci. Total Environ.* 565 (2015) 889–901. doi:10.1016/j.scitotenv.2016.02.003.
- [26] R.M. Moattari, S. Rahimi, L. Rajabi, A.A. Derakhshan, M. Keyhani, Statistical investigation of lead removal with various functionalized carboxylate ferroxane nanoparticles, *J. Hazard. Mater.* 283 (2015) 276–291. doi:10.1016/j.jhazmat.2014.08.025.
- [27] F. Fu, D.D. Dionysiou, H. Liu, The use of zero-valent iron for groundwater remediation and wastewater treatment: A review, *J. Hazard. Mater.* 267 (2014) 194–205. doi:10.1016/j.jhazmat.2013.12.062.
- [28] M. Stefaniuk, P. Oleszczuk, Y.S. Ok, Review on nano zerovalent iron (nZVI): From synthesis to environmental applications, *Chem. Eng. J.* 287 (2016) 618–632. doi:10.1016/j.cej.2015.11.046.

- [29] R. Singh, V. Misra, R.P. Singh, Removal of Cr(VI) by nanoscale zero-valent iron (nZVI) from soil contaminated with tannery wastes, *Bull. Environ. Contam. Toxicol.* 88 (2012) 210–214. doi:10.1007/s00128-011-0425-6.
- [30] C. Fajardo, M. Gil-Díaz, G. Costa, J. Alonso, A.M. Guerrero, M. Nande, M.C. Lobo, M. Martín, Residual impact of aged nZVI on heavy metal-polluted soils, *Sci. Total Environ.* 535 (2015) 79–84. doi:10.1016/j.scitotenv.2015.03.067.
- [31] X. Qiu, Z. Fang, X. Yan, F. Gu, F. Jiang, Emergency remediation of simulated chromium (VI)-polluted river by nanoscale zero-valent iron: Laboratory study and numerical simulation, *Chem. Eng. J.* 193–194 (2012) 358–365. doi:10.1016/j.cej.2012.04.067.
- [32] V. Tanboonchuy, N. Grisdanurak, C.-H. Liao, Background species effect on aqueous arsenic removal by nano zero-valent iron using fractional factorial design, *J. Hazard. Mater.* 205 (2012) 40–46. doi:10.1016/j.jhazmat.2011.11.090.
- [33] R.A. Crane, T.B. Scott, Nanoscale zero-valent iron: Future prospects for an emerging water treatment technology, *J. Hazard. Mater.* 211 (2012) 112–125. doi:10.1016/j.jhazmat.2011.11.073.
- [34] S.R. Kanel, B. Manning, L. Charlet, H. Choi, Removal of Arsenic (III) from Groundwater by Nanoscale Zero-Valent Iron, *Environ. Sci. Technol.* 39 (2005) 1291–1298. doi:10.1021/es048991u.
- [35] R. Rangsvivek, M.R. Jekel, Removal of dissolved metals by zero-valent iron (ZVI): Kinetics, equilibria, processes and implications for stormwater runoff treatment, *Water Res.* 39 (2005) 4153–4163. doi:10.1016/j.watres.2005.07.040.
- [36] D. O’Carroll, B. Sleep, M. Krol, H. Boparai, C. Kocur, Nanoscale zero valent iron and bimetallic particles for contaminated site remediation, *Adv. Water Resour.* 51 (2013) 104–122. doi:10.1016/j.advwatres.2012.02.005.
- [37] G.Z. Kyzas, K.A. Matis, Nanoadsorbents for pollutants removal: A review, *J. Mol. Liq.* 203 (2015) 159–168. doi:10.1016/j.molliq.2015.01.004.
- [38] C. Sierra, D. Martínez-Blanco, J. a Blanco, J.R. Gallego, Optimisation of magnetic separation: A case study for soil washing at a heavy metals polluted site., *Chemosphere.* (2014). doi:10.1016/j.chemosphere.2013.12.063.
- [39] J. Svoboda, T. Fujita, Recent developments in magnetic methods of material separation, *Miner. Eng.* 16 (2003) 785–792. doi:10.1016/S0892-6875(03)00212-7.
- [40] F. Lotze, Zur Gliderung der Varisziden der Iberischen Meseta, *Geotekt. Forsch.* 6 (1945)

78–92.

- [41] M. Julivert, A. Marcos, Superimposed folding under flexural conditions in the Cantabrian Zone (Hercynian Cordillera, northwest Spain), *Am. J. Sci.* 273 (1973) 353–375. doi:10.2475/ajs.273.5.353.
- [42] C. Luque, M. Gutierrez-Claverol, *La minería del mercurio en Asturias. Rasgos históricos.*, 2006.
- [43] M. Gil-Díaz, J. Alonso, E. Rodríguez-Valdés, P. Pinilla, M.C. Lobo, Reducing the mobility of arsenic in brownfield soil using stabilised zero-valent iron nanoparticles., *J. Environ. Sci. Health. A. Tox. Hazard. Subst. Environ. Eng.* 49 (2014) 1361–9. doi:10.1080/10934529.2014.928248.
- [44] G. Mercier, J. Duchesne, D. Blackburn, Prediction of metal removal efficiency from contaminated soils by physical methods., *J. Environ. Eng. (Reston, Virginia)*. 127 (2001) 348–358.
- [45] L. Ma, Q. Yang, Y. Huang, P. Qian, J.G. Wang, Pilot Test on the Removal of Coke Powder from Quench Oil Using a Hydrocyclone, *Chem. Eng. Technol.* 36 (2013) 696. <http://onlinelibrary.wiley.com/doi/10.1002/ceat.201200316/abstract>.
- [46] Q. Yang, Z.M. Li, W.J. Lv, H.L. Wang, On the laboratory and field studies of removing fine particles suspended in wastewater using mini-hydrocyclone, *Sep. Purif. Technol.* 110 (2013) 93–100. doi:10.1016/j.seppur.2013.03.025.
- [47] D.J. Nieuwoudt, J.S.J. Van Deventer, M.A. Reuter, V.E. Ross, The influence of design variables on the flotation of pyrite in an air-sparged hydrocyclone, *Miner. Eng.* 3 (1990) 483–499. doi:10.1016/0892-6875(90)90041-9.
- [48] C. Boente, C. Sierra, E. Rodríguez-Valdés, J.M. Menéndez-Aguado, J.R. Gallego, Soil washing optimization by means of attributive analysis: Case study for the removal of potentially toxic elements from soil contaminated with pyrite ash, *J. Clean. Prod.* (2016). doi:10.1016/j.jclepro.2016.11.007.
- [49] A.G. Caporale, A. Violante, Chemical Processes Affecting the Mobility of Heavy Metals and Metalloids in Soil Environments, *Curr. Pollut. Reports.* 2 (2016) 15–27. doi:10.1007/s40726-015-0024-y.
- [50] M.B. Ogundiran, O. Osibanjo, Mobility and speciation of heavy metals in soils impacted by hazardous waste, *Chem. Speciat. Bioavailab.* 21 (2009) 59–69. doi:10.3184/095422909X449481.
- [51] L. Giraldo, A. Erto, J.C. Moreno-Piraján, Magnetite nanoparticles for removal of heavy

- metals from aqueous solutions: Synthesis and characterization, in: *Adsorption*, 2013: pp. 465–474. doi:10.1007/s10450-012-9468-1.
- [52] X.S. Wang, H.J. Lu, F. Liu, J.J. Ren, Adsorption of lead(II) ions onto magnetite nanoparticles, *Adsorpt. Sci. Technol.* 26 (2011) 407–417.
- [53] I. Carabante, Arsenic (V) Adsorption on Iron Oxide, Implication for Soil Remediation and Water Purification. (2012).
- [54] S. Fendorf, P.S. Nico, B.D. Koncar, Y. Massue, K.J. Tufano, Arsenic Chemistry in Soils and Sediments, Lawrence Berkeley Natl. Lab. (2010).
- [55] C.H. Liu, Y.H. Chuang, T.Y. Chen, Y. Tian, H. Li, M.K. Wang, W. Zhang, Mechanism of Arsenic Adsorption on Magnetite Nanoparticles from Water: Thermodynamic and Spectroscopic Studies, *Environ. Sci. Technol.* 49 (2015) 7726–7734. doi:10.1021/acs.est.5b00381.
- [56] S. Dixit, J. Hering, Comparison of arsenic (V) and arsenic (III) sorption onto iron oxide minerals: Implications for arsenic mobility, *Environ. Sci. Technol.* 37 (2003) 4182–4189. doi:10.1021/es030309t.
- [57] S.M. Shaheen, C.D. Tsadilas, J. Rinklebe, A review of the distribution coefficients of trace elements in soils: Influence of sorption system, element characteristics, and soil colloidal properties, *Adv. Colloid Interface Sci.* 201–202 (2013) 43–56. doi:10.1016/j.cis.2013.10.005.
- [58] H.L. Anderson, S.D. Balsley, P.V. Brady, Iodide retention by cinnabar (HgS) and chalcocite (Cu<sub>2</sub>S), Sandia Natl. Labs. No. SAND, (1995).
- [59] P. Somasundaran, K.P. Ananthapadmanabhan, *Handbook of Separation Process Technology*. (1987) 775-805.

## Tables

**Table 1. Particle-size distribution and element concentration of the bulk and initial grain-size fractions (aqua-regia digestion and ICP-OES analysis).**

Grain-size fraction ( $\mu\text{m}$ )	Weight (%)	Element concentration											
		Al (%)	As (ppm)	Ca (%)	Cu (ppm)	Fe (%)	Hg (ppm)	K (%)	La (ppm)	Pb (ppm)	Sb (ppm)	V (ppm)	Y (ppm)
> 2000	50.4	-	-	-	-	-	-	-	-	-	-	-	-
500–2000	11.0	0.6	182.4	2.8	92.6	1.0	73.7	0.3	14.4	22.4	10.4	11.4	15.9
125–500	12.6	0.5	123.0	1.6	63.7	0.9	53.5	0.2	10.3	52.1	9.3	9.8	15.3
< 125	25.9	0.9	380.7	1.6	300.5	2.6	153.8	0.2	17.4	129.4	18.2	24.7	29.5
Bulk	-	0.7	249.0	2.4	88.0	1.6	100.6	0.3	14.0	46.0	13.0	17.0	23.0

**Table 2. Results for WHIMS experiments.  $WR_c^i$  designates the corrected weight recovery in the concentrated fraction and  $ER_c^i$  the corrected element recoveries for PTEs. In the case of Fe, uncorrected  $ER_{ic}$  values had to be used. Results correspond to the average of three measurements with a standard error < 3%.**

Grain-size fraction ( $\mu\text{m}$ )	WHIMS Voltage (% of the maximum output)	Soil washing							nZVI-assisted soil washing						
		$WR_c^i$ (%)	$ER_c^i$	$ER_c^i$					$WR_c^i$ (%)	$ER_c^i$	$ER_c^i$				
				Fe	As	Cu	Hg	Pb			Sb	Fe	As	Cu	Hg
500–2000	10	8	3.22	24	19	4	14	18	55	14.30	59	76	37	62	61
	20	14	2.85	35	25	9	16	29	60	18.00	66	78	66	82	71
	30	17	3.17	41	40	6	36	38	69	14.10	75	94	45	86	82
	50	20	3.21	49	41	7	43	45	76	7.07	80	92	46	87	82
125–500	10	5	3.96	16	17	2	25	17	30	25.70	31	78	10	36	45
	20	6	4.10	20	13	3	20	20	43	21.70	44	85	21	50	60
	30	8	4.25	28	22	4	30	27	37	20.40	41	81	19	49	55
	50	10	4.14	36	30	5	40	31	51	20.90	56	89	27	62	70
< 125	10	3	7.24	9	8	4	11	12	35	21.80	37	59	39	42	43
	20	6	7.68	18	14	6	24	22	47	20.10	51	68	48	55	56
	30	7	7.41	17	14	7	19	22	60	17.40	60	75	65	66	67
	50	8	7.13	20	16	8	22	25	51	22.00	54	74	49	57	61



**Table 3. Results for hydrocycloning experiments for the < 125  $\mu\text{m}$  fraction under different conditions.  $\text{WR}_c'$  indicates the corrected weight recovery in the concentrated fraction.  $\text{ER}_c^i$  represents the corrected element recoveries for PTEs except for Fe (uncorrected). Results correspond to the average of three measurements with a standard error < 3%.**

Assay conditions		Soil washing						nZVI-assisted soil washing							
Apex diameter (mm)	Pressure (kPa)	$\text{WR}_c'$	$\text{ER}_c^i$ (%)		$\text{ER}_c^i$ (%)				$\text{WR}_c'$	$\text{ER}_c^i$ (%)		$\text{ER}_c^i$ (%)			
			Fe	As	Cu	Hg	Pb	Sb		Fe	As	Cu	Hg	Pb	Sb
6.4	68.95	18	5,32	27	31	20	33	25	38	21,30	46	60	37	51	45
6.4	137.90	22	5,37	33	41	27	40	30	25	21,40	31	43	24	35	33
9.5	68.95	16	5,30	26	28	20	31	24	28	21,50	31	44	24	38	35
9.5	137.90	12	5,48	16	20	15	23	19	25	21,70	31	40	22	33	30

**Table 4. nZVI concentration derived from M(H) curves.  $\%_M^{\text{nZVI}}$  and  $\%_{\text{NM}}^{\text{nZVI}}$  are the percentages of nZVI in the mags and non-mags fractions, respectively,  $\%_M$  is the proportion of magnetics in the mags fraction, and  $\%_s^{\text{nZVI}}$  is the percentage of nZVI in each feed, calculated by means of equation 8.**

Voltage (% of the maximum output)	2000–500- $\mu\text{m}$				125–500 $\mu\text{m}$				< 125 $\mu\text{m}$			
	$\%_M^{\text{nZVI}}$	$\%_{\text{NM}}^{\text{nZVI}}$	$\%_M$	$\%_s^{\text{nZVI}}$	$\%_M^{\text{nZVI}}$	$\%_{\text{NM}}^{\text{nZVI}}$	$\%_M$	$\%_s^{\text{nZVI}}$	$\%_M^{\text{nZVI}}$	$\%_{\text{NM}}^{\text{nZVI}}$	$\%_M$	$\%_s^{\text{nZVI}}$
10	18.44	0.14	89.42	16.51	22.24	0.41	49.75	11.27	28.98	0.82	62.86	18.52
20	18.26	0.28	90.24	16.48	27.84	0.31	39.81	11.08	32.23	0.95	56.17	18.11
30	39.52	0.00	41.81	16.52	38.79	0.31	28.48	11.05	26.51	0.64	69.11	18.32
50	27.13	0.06	60.76	16.48	33.44	0.10	33.50	11.20	31.81	0.71	57.27	18.22

## Figures

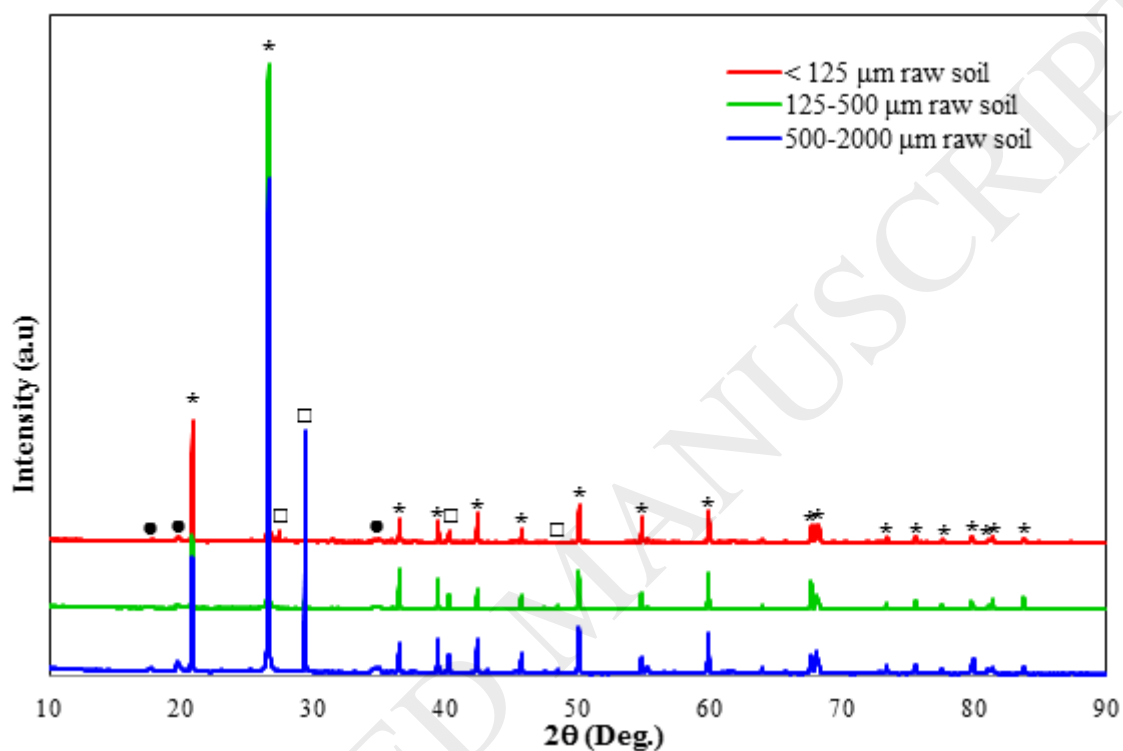
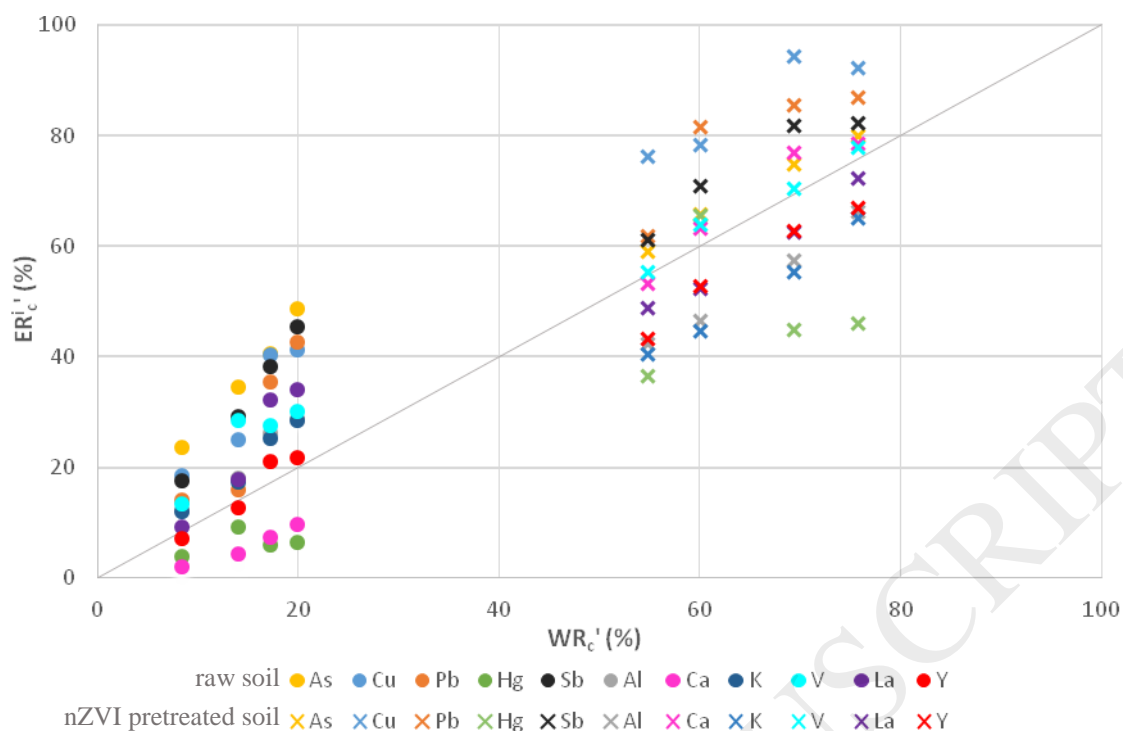
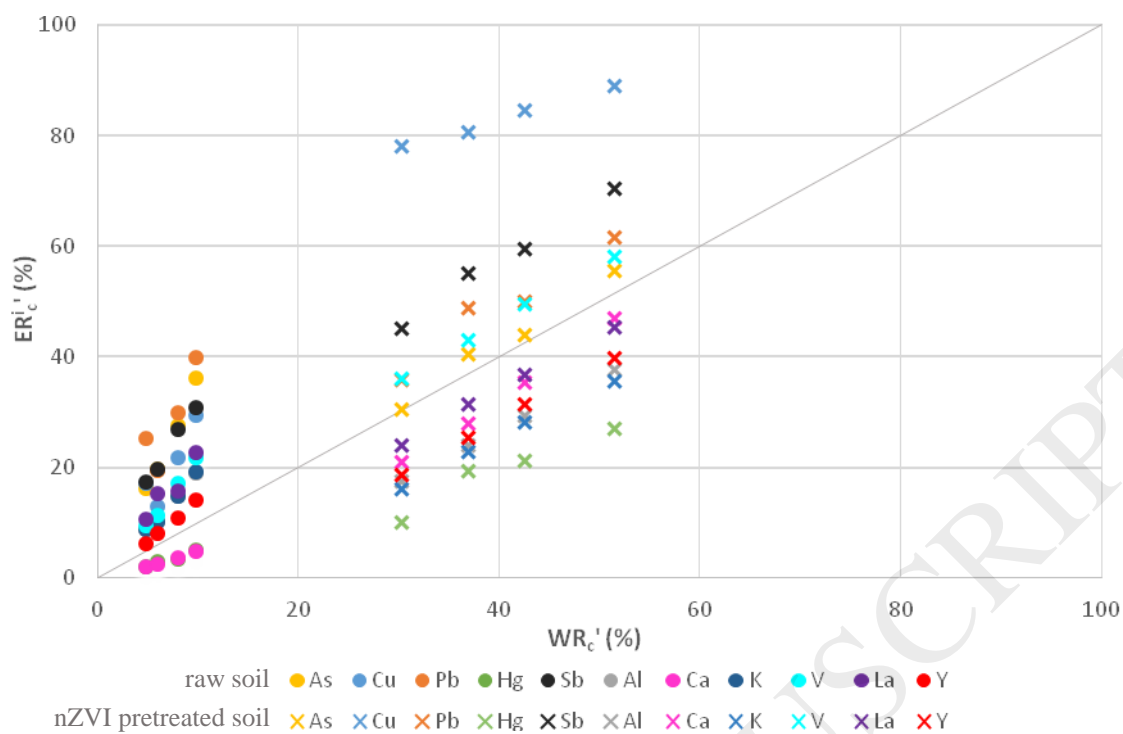


Fig. 1. X-ray diffraction patterns for the raw soil of grain size: 500–2000  $\mu\text{m}$  (blue), 125–500-  $\mu\text{m}$  (green) and  $< 125 \mu\text{m}$  (red). Characteristic peaks of main crystalline phases identified are indicated as: quartz (\*), calcite (□) and muscovite (●).



**Fig. 2.** Corrected element recovery vs. corrected weight recovery for the 500–2000  $\mu\text{m}$  fraction after WHIMS. Crosses and circles and represent experiments with and without nZVI pretreatment, respectively. Vertical alignments correspond, from left to right, to increasing output voltages.



**Fig. 3.** Corrected element recovery vs. corrected weight recovery for the 125–500  $\mu\text{m}$  fraction after WHIMS. Crosses and circles and represent experiments with and without nZVI pretreatment, respectively. Vertical alignments correspond, from left to right, to increasing output voltages.

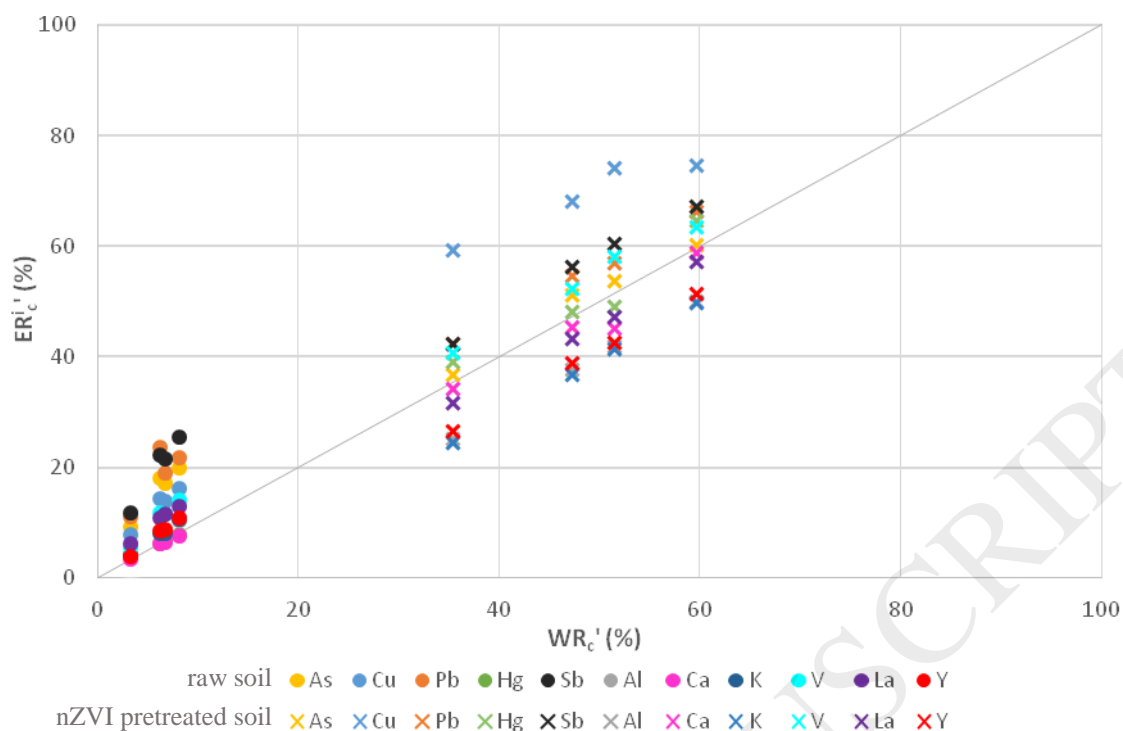


**Fig. 4. Corrected element recovery vs. corrected weight recovery for the < 125  $\mu\text{m}$  fraction after WHIMS. Crosses and circles represent experiments with and without nZVI pretreatment, respectively. Vertical alignments correspond, from left to right, to increasing output voltages.**

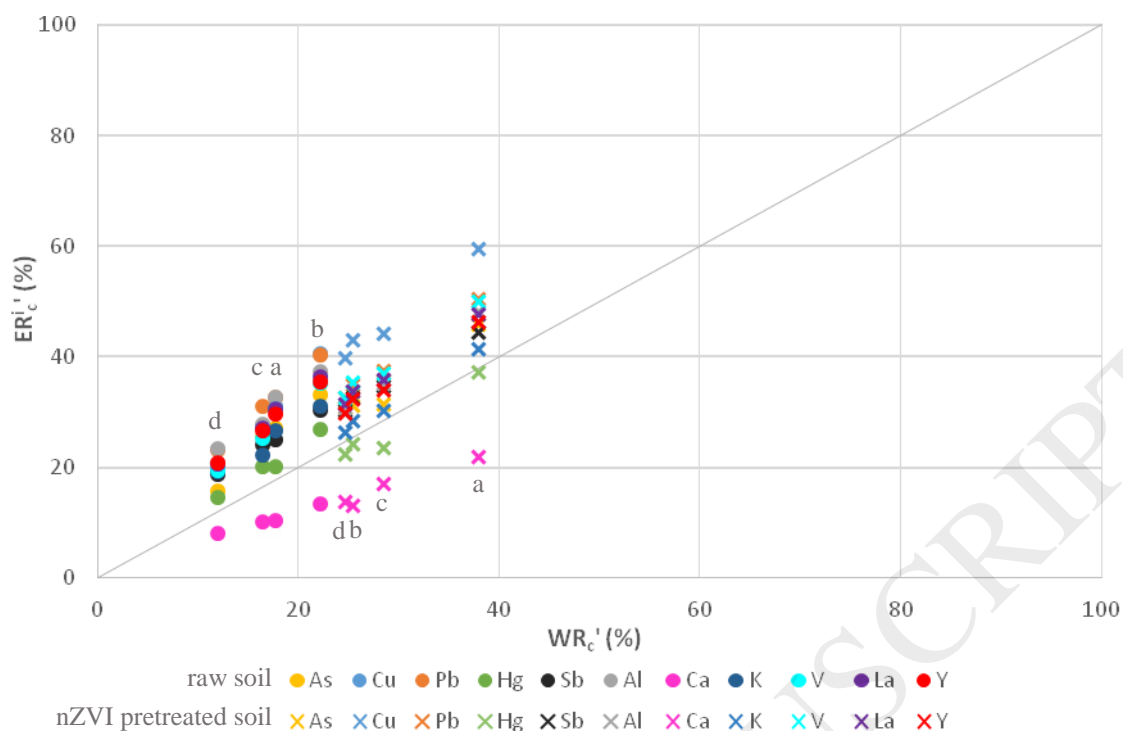


**Fig. 5. Corrected element recovery vs. corrected weight recovery for the < 125  $\mu\text{m}$  fraction after treatment with the hydrocyclone. Crosses and circles and represent experiments with and without nZVI pretreatment, respectively. Vertical alignments correspond to a) 6.4 mm apex diameter and 68.95 kPa; b) 6.4 mm apex diameter and 137.90 kPa; c) 9.5 mm apex diameter and 68.95 kPa; d) 9.5 mm apex diameter and 137.90 kPa.**

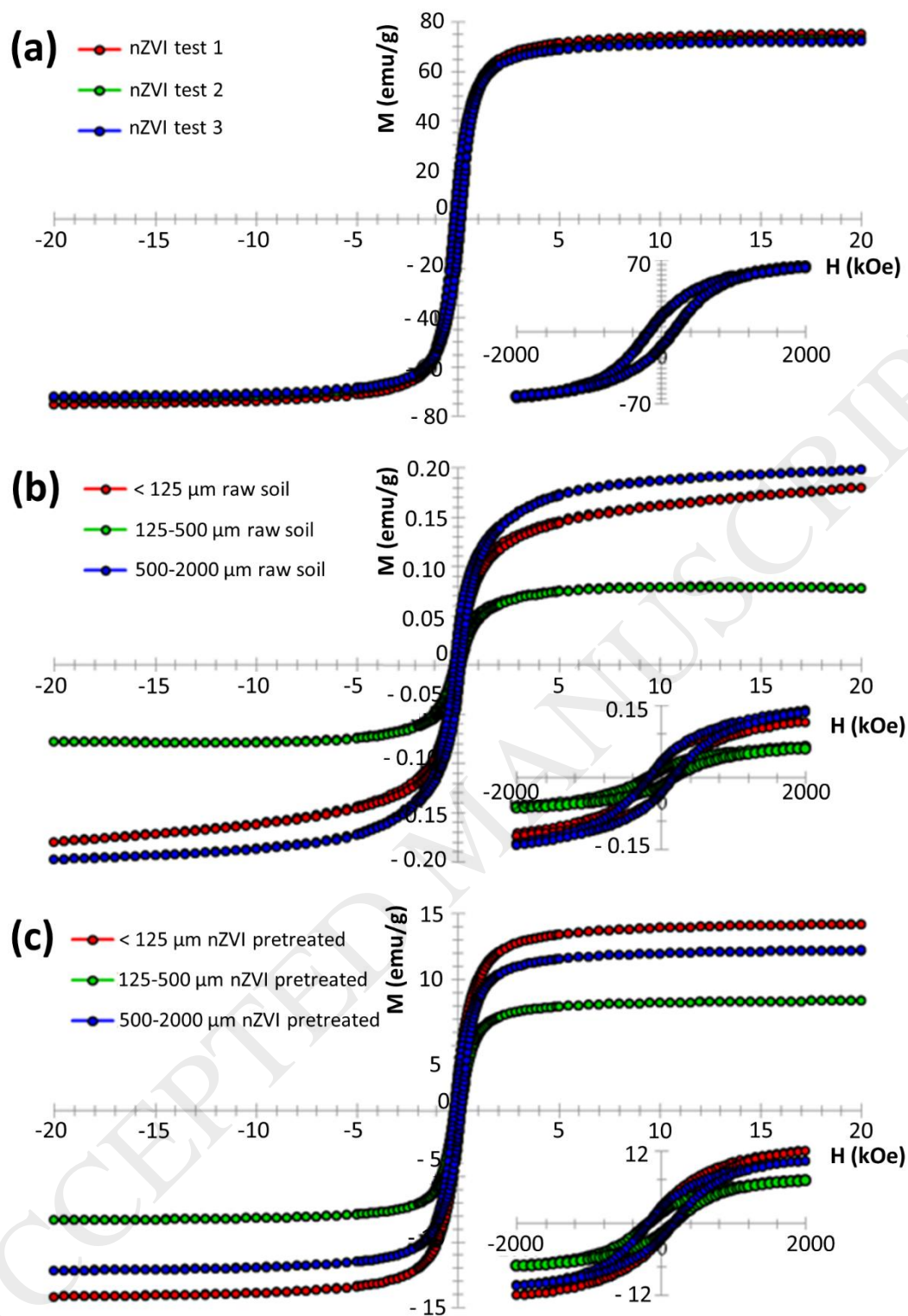


**Fig. 6.** Hysteresis loops of: a) pure nZVI, b) raw soil, and (c) nZVI pretreated soil.  $M$ , is the specific magnetization; and  $H$ , the magnetic field applied. Grain size: 500–2000  $\mu\text{m}$  (blue), 125–500-  $\mu\text{m}$  (green) and <math>< 125 \mu\text{m}</math> (red). Bottom right loops indicate the magnification of the central section of the loop.

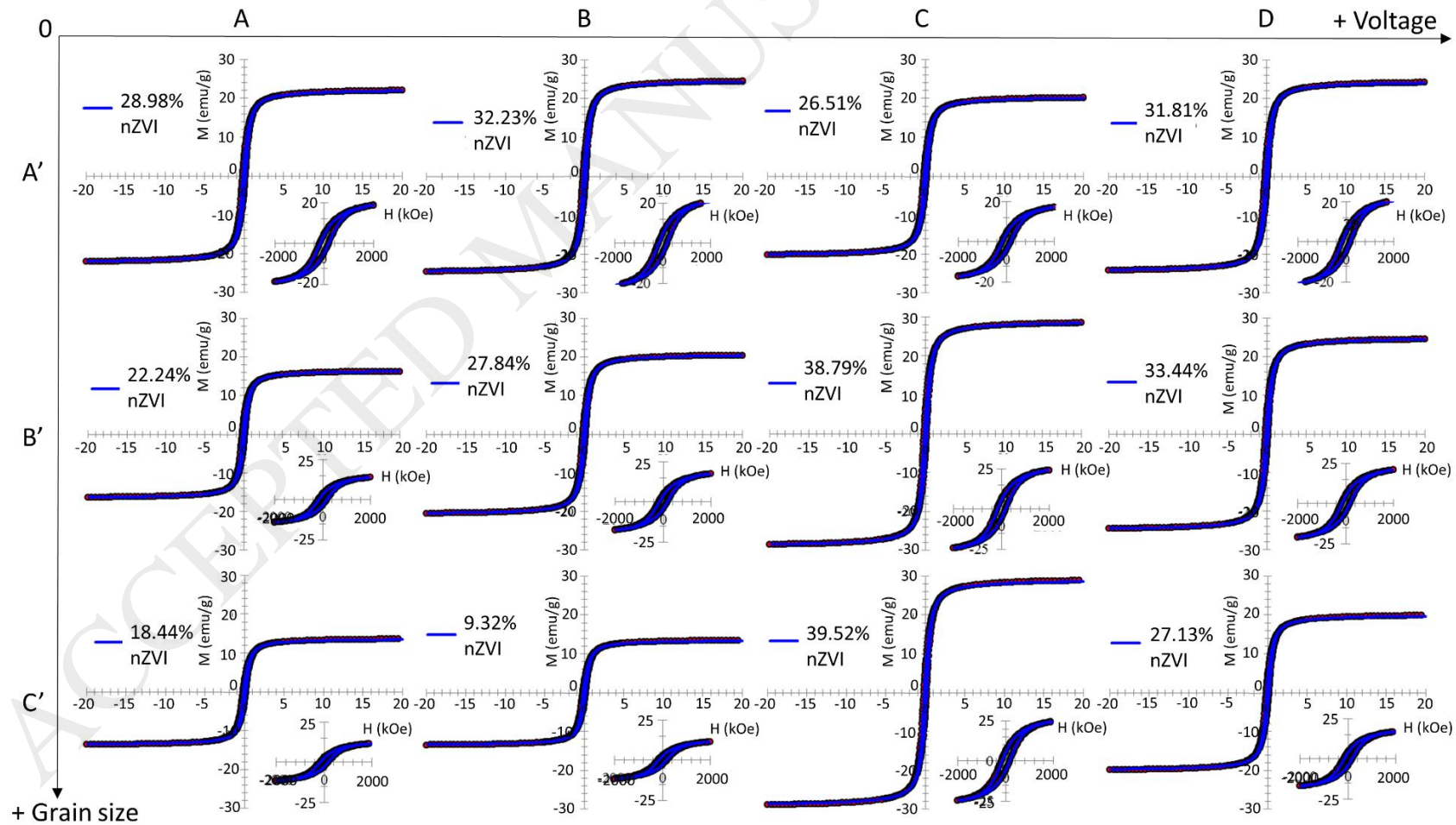


**Fig. 7.** M(H) curves for magnetic fractions of the feeds after WHIMS. Hysteresis loops are arranged in rows by grain size: A':  $< 125 \mu\text{m}$ , B':  $125\text{--}500 \mu\text{m}$  and C':  $500\text{--}2000 \mu\text{m}$ ; and in columns by percentages of maximum output voltage: A (10%), B (20%), C (30%) and D (50%). Bottom right loops are the magnification of the central section of the loop. % values correspond to the weight % of nZVI in the mags fraction.



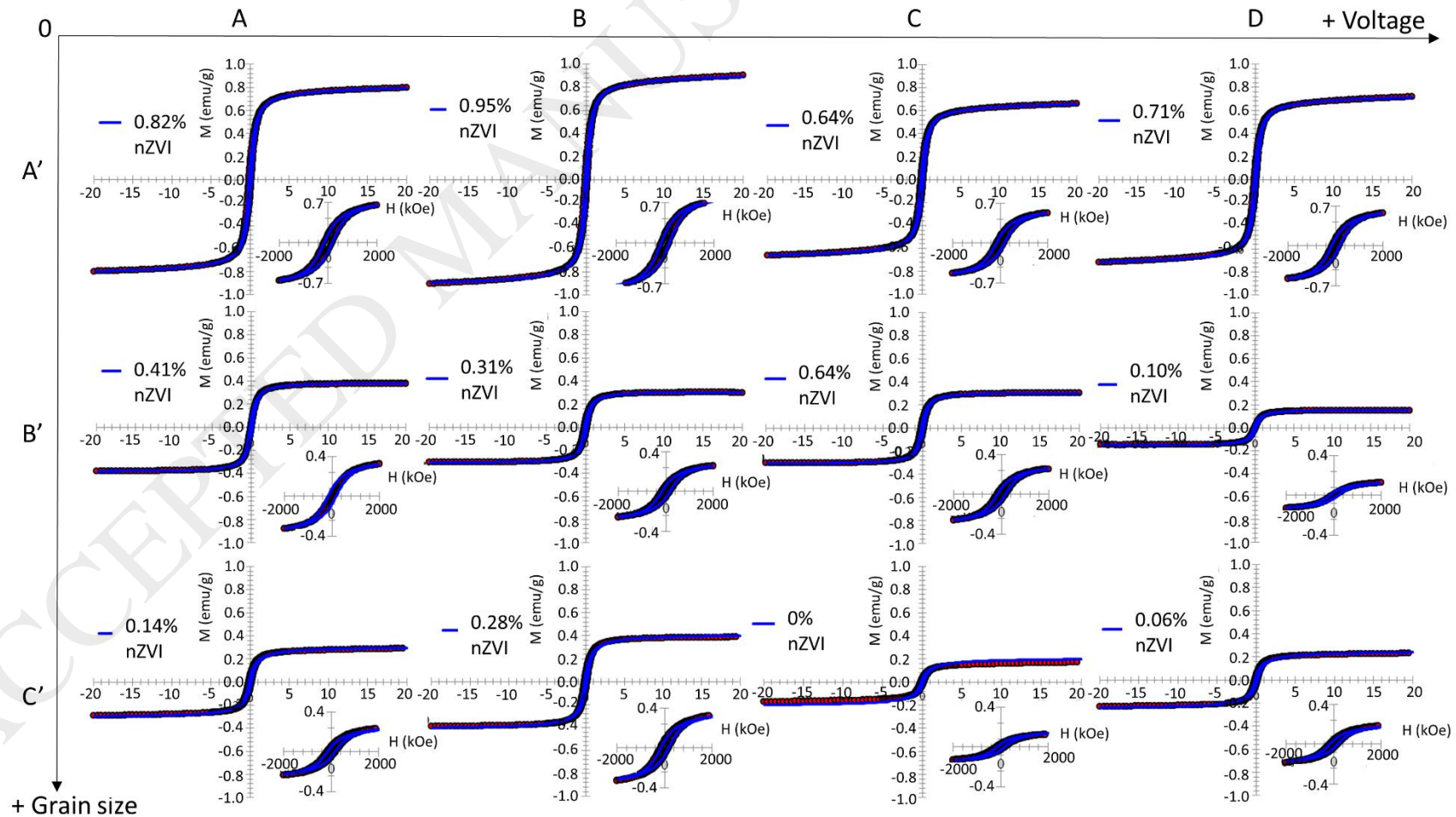


Fig. 8.  $M(H)$  curves for non-magnetic fractions of the feeds after WHIMS. Hysteresis loops are arranged in rows by grain size: A':  $< 125 \mu\text{m}$ , B':  $500\text{--}125 \mu\text{m}$  and C':  $500\text{--}2000 \mu\text{m}$ ; and in columns by percentages of maximum output voltage: A (10%), B (20%), C (30%) and D (50%). Bottom right loops are the magnification of the central section of the loop. % values correspond to the weight % of nZVI in the non-mag fraction.